University of Groningen

Upscaling, integration and electrical characterization of molecular junctions

Van Hal, Paul A.; Smits, Edsger C. P.; Geuns, Tom C. T.; Akkerman, Hylke B.; De Brito, Bianca C.; Perissinotto, Stefano; Lanzani, Guglielmo; Kronemeijer, Auke J.; Geskin, Victor; Cornil, Jerome

IMPORTANT NOTE: You are advised to consult the publisher's version (publisher's PDF) if you wish to cite from it. Please check the document version below.

Document Version
Publisher's PDF, also known as Version of record

[Link to publication in University of Groningen/UMCG research database](#)

Upscaling, integration and electrical characterisation of molecular junctions

Paul A. van Hal, Edsger C. P. Smits, Tom C. T. Geuns, Hylke B. Akkerman, Bianca C. de Brito, Stefano Perissinotto, Guglielmo Lanzani, Auke J. Kronemeijer, Victor Geskin, Jérôme Cornil, Paul W. M. Blom, Bert de Boer, and Dago M. de Leeuw

Supplementary information

Contents

1. Summary

This Supplementary Information presents the details on preparation and characterisation of molecular junctions and serial integration thereof. The detailed information is included to allow other research groups to reproduce the experimental data, and to support the presented interpretation.
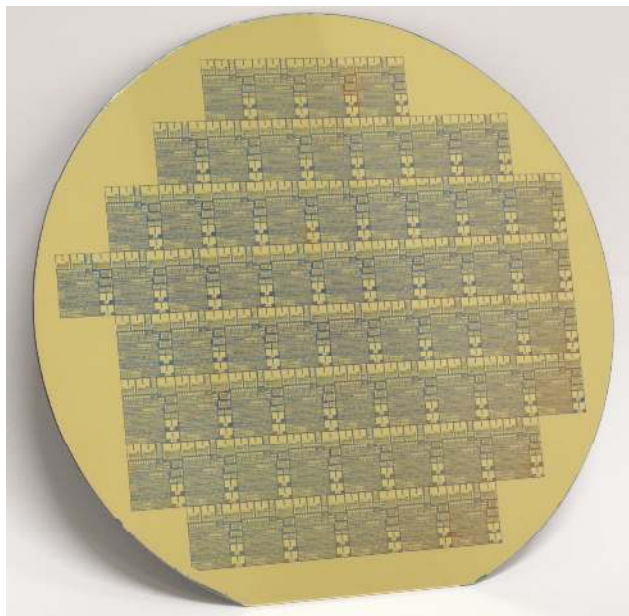
Fig. S1. Photograph of a finished 150-mm wafer. Each wafer contains 62 dies comprising thousands of molecular junctions. The process evaluation module (PEM) allows automatic measurement of e.g. sheet resistances, leakage currents, capacitances, and contact resistances of discrete molecular junctions and strings of junctions connected in series.

A photograph of a finished wafer is presented in Fig. S1. The methods are presented in the experimental part, section 2. The electrical transport perpendicular through a self-assembled-monolayer (SAM) sandwiched between two electrodes is investigated. The junctions are processed in vertical interconnects, *via's,* enclosed in photoresist to prevent cross talk. The technology to fabricate the molecular junctions on 150-mm wafers is presented in section 3. We start with the fabrication of the first electrode that contains the bottom contact and the first layer of interconnects. Then the *via* definition is described, followed by the SAM formation. XPS, contact angle and workfunction measurements confirm densely packed SAMs. The second electrode layer consists of a stack of the conducting polymer PEDOT:PSS and gold. The PEDOT:PSS is inserted to prevent top-down shorts during gold evaporation. In this electrode layer the top contacts and second layer of interconnects are defined. The lithography and subsequent process steps have been performed at room temperature. Finally the device geometries are presented. To eliminate lead resistances 4 point probe Kelvin structures have been used. Process integration is demonstrated in strings in which up to 200 molecular junctions are connected in series. The leakage currents are addressed and shown to be negligible.

In section 4 we present additional information on the electrical transport measurements of molecular junctions. First PEDOT:PSS-only junctions are addressed. As a typical example we present detailed current-voltage characteristics of alkane-mono-thiol SAM junctions. A statistical analysis of thousands of junctions is presented. Key parameters as yield and reproducibility are given. The scaling of resistance with device area is discussed and the influence of process parameters on the resistance of the molecular junctions is given.

2. Experimental

The molecular junctions were fabricated in a class 1000 clean room of MiPlaza at High Tech Campus in Eindhoven. Metal electrodes were applied either by sputtering using a CVC Connexion 800 sputter unit or by evaporation using a Balzers BAK-550 evaporator. Electrodes were patterned by I-line projection photolithograpy using an ASML PAS5500/100 stepper. The negative epoxy-based photoresists MA1407 and L6000.5 and the corresponding developers MA-D 533S and M600 were purchased from Micro Resist Technology GmbH (Germany) and Microchem (Germany), respectively. Layer thicknesses were measured with an optical profilometer or with a DEKTAK surface profilometer. PEDOT:PSS is structured with reactive ion etching using a STS Multiplex Clustertool.

The series of alkane-mono-thiol C_nH_{2n+1}-SH with n = 8-18 and the compound HS-C_8H_{16}-SH were purchased from Sigma-Aldrich. C_nH_{2n+1}-SH with n = 20 was obtained from Robinson Brothers Ltd (U.K.). C_nH_{2n+1}-SH with n = 22 and a series α,ω-alkane-di-thiols HS-C_nH_{2n}-SH with n = 10, 12, 14, 16 were synthesized according to literature procedures[1]. Water borne PEDOT:PSS suspensions were obtained from Agfa Gevaert N.V. (ORGACON) and from H.C. Starck (CLEVIOS). The non ionic surfactant, $F(CF_2CF_2)_x(CH_2CH_2O(CH_2CH_2O)_y$ H with x = 1-7; y = 0-15 (Zonyl FSO-100) was obtained from Dupont. All solvents used, *i.e.* ethanol, toluene, iso-propanol and acetone, were purchased from Aldrich.

SAMs and molecular junctions were characterised with various analytical techniques. X-ray Photoelectron Spectroscopy (XPS) measurements have been carried out in a Quantum 2000 spectrometer from ULVAC-PHI. Atomic Force Microscopy (AFM) measurements were performed with a Veeco Dimension 3100 atomic force microscope equipped with a Nanoscope IV control unit. Workfunctions were measured using a Kelvin Probe from Besocke Delta Phi. Freshly cleaved HOPG was used a reference with its workfunction in air taken as 4.48 eV [2]. Ellipsometry measurements were performed on a J.A. Woollam Co., Inc Spectroscopic Ellipsometer, VB-400. The measurements were performed in ambient conditions using a wavelength range between 300-800 nm at incidence angles of 65, 70 and 75 degrees. For the interpretation we took a refractive index for the alkanethiols of 1.45[3]. Furthermore the SAM layers on Au were modelled using a Cauchy layer on top of Au. Cross sections of molecular junctions were made with a focused ion beam, FIB200. A 1 μm Pt layer is deposited on the region of interest to protect the sample during focussed ion beam milling. Using 30 keV Ga-ions a hole is milled in the surface with one steep edge oriented perpendicular to the sample surface, and a step like construction at the opposite side. Transmission electron microscopic (TEM) studies were performed using a TECNAI F30ST TEM operated at 300 kV. By tilting the sample at an angle of 45° an image of the chemical composition is formed by

detection of the secondary electrons. The SAM layer cannot be resolved. The chemical composition was obtained using energy selective filters. Contact angle measurements were performed to characterise the hydrophobicity of the SAMs. Advancing and receding contact angles were measured with HPLC grade water as the drop phase.

Each processed wafer contained 62 dies. The process evaluation module (PEM) used allowed for measurement of *e.g.* sheet resistances, leakage currents, contact resistances, strings of junctions in series and capacitances. The devices were measured with an Electroglass semi-automatic prober using a POLPEM16 probe card. Each die contained eight 4-point probe Kelvin structures[4] to measure the Au / SAM / PEDOT:PSS / Au resistance. The diameter of the circular *vias* ranged from 1 to 50 μm. The resistance was measured in ambient conditions at 0.5 V bias. In total each wafer yielded about 500 discrete junctions and 20000 serially integrated molecular junctions.

Discrete junctions were measured as function of bias and ambient using an Agilent 4155C semiconductor parameter analyzer. In agreement with literature reports[5] we found that the presence of water can easily lead to erroneous artefacts such as negative differential resistances. In ambient conditions the junctions are stable up to about 1 V. At higher bias, typically 2 V, electrolysis occurs at the PEDOT electrode. Gasses formed cannot escape because the junctions are enclosed in photoresist and sandwiched between a top and bottom electrode. The pressure rises, the PEDOT:PSS delaminates, the electrical contact is lost and the resistance increases by many orders of magnitude. Details are presented elsewhere[6]. In high vacuum the resistance is typically larger by a factor of three. The junctions can then be measured up to 3 V without any hysteresis or deterioration. Using low duty cycle pulse measurements, not further discussed here, the junctions can even be characterised up to 10 V bias. The wafers are stored in air. Over periods of months there is no change in resistance.

3. Process technology

The process flow chart is schematically presented in Fig. S2. A gold electrode is deposited on a 150-mm substrate and patterned by photolithography to obtain the bottom contacts and the first layer of interconnects. To electrically isolate the junctions they are processed in vertical interconnects defined in photoresist. After developing the photoresist and cleaning of the gold, an alkane(di)thiol monolayer is self-assembled from an ethanolic solution. Alkane(di)thiols are used to benchmark the resistances versus literature data. On top of the SAM a thin layer of PEDOT:PSS is spin coated. After drying the gold top electrode is applied. The electrically conducting PEDOT:PSS layer prevents the formation of top down-shorts. The difference in surface tension between the hydrophobic SAM and the waterborne PEDOT:PSS prevents mixing thereof. The gold top contacts and the second layer of interconnects are defined in the top gold electrode by photolithography and dry etching. Finally, the PEDOT:PSS outside the junctions is removed by RIE etching using the patterned top gold contacts as a self-aligned mask. In this section details of the process technology are presented.
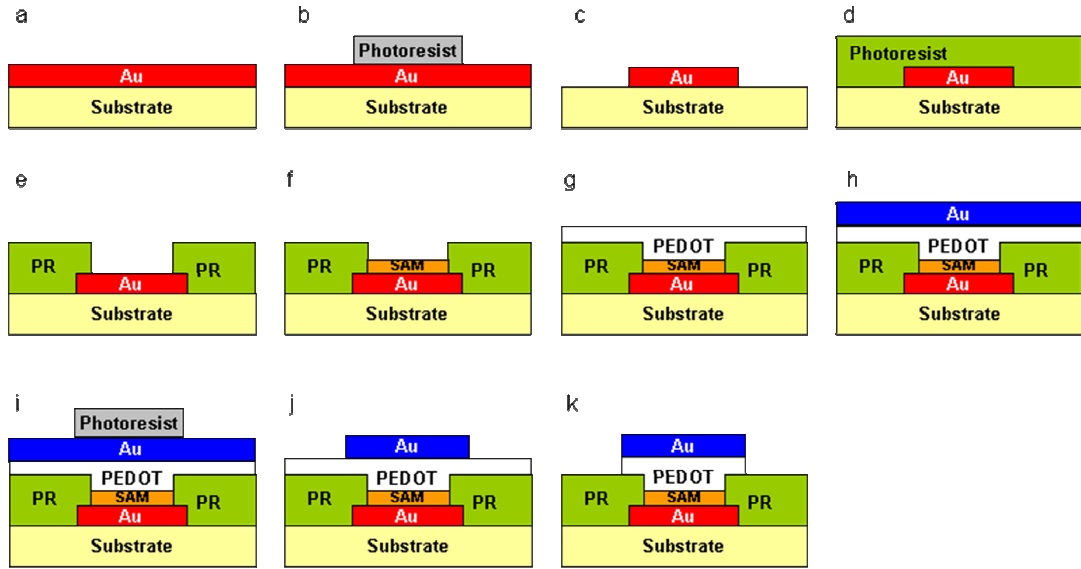
Fig. S2. Schematic representation of the process flow chart. (a) deposition of Au bottom electrode; (b,c) patterning Au bottom electrode using photolithography; (d) spin coating of negative photoresist; (e) photolithographical definition of vertical interconnect; (f) SAM formation; (g) spin coating of PEDOT:PSS; (h) deposition Au top electrode; (i, j) patterning Au top electrode using photolithography; (k) self-aligned removal of PEDOT:PSS outside of the junction area.

Bottom electrode and via definition

A 150-mm c-Si monitor wafer with a 1 μm thermally grown SiO_2 layer was used as substrate. The bottom electrode consisted of a 50 nm sputtered Au electrode. As an adhesion layer 2 nm Ti was used. The surface roughness increased with layer thickness. The root mean square roughness for a 50 nm Au film amounted to 0.7 nm. A doubled surface roughness by increasing the layer thickness to 150 nm did not change the resistances of the final molecular junctions. The use of Cr as an adhesion layer yielded slightly different resistances, the reason of which is not exactly understood.

The bottom contacts and the first layer of interconnect were defined by I-line projection photolithography using HPR as a positive photoresist. After exposure and developing the Au was etched in a KI/I_2 (1:1) solution in water. The Ti was wet etched using a HNO_3/HF solution. The protecting photoresist was then stripped with acetone. Organic residues were removed with fuming HNO_3, and washed away with de-ionised water.

The junctions were fabricated in vertical interconnects (*via*) defined in 500 nm photoresist. The diameter of the circular *vias* ranged from 1 to 50 μm. We examined two different photoresists, MA1407 and L6000.5. In order to adhere MA1407, the wafer was first passivated with hexamethyldisilazane (HMDS). After spinning and exposure, the MA1407 photoresist was developed in aqueous media. The patterned photoresist was baked at 200 °C in vacuum for 1 hour to make the wafer solvent resistant. XPS measurements showed the presence of Ti at the Au bottom electrode

when using a post-bake step above 150 °C. To reduce the post bake temperature we used the photoresist L6000.5. This resist can be directly applied on the substrate and HMDS passivation is not needed. After exposure and a 5 minute post-exposure bake step at 95 °C, the resist was developed in organic media and hard baked for 2 minutes at 140 °C. At this temperature Ti is not observed by XPS measurements. We note that the surface roughness did not change during the post bake steps.

After the *via* definition still some organic residues are left on the Au bottom electrode. These contaminants were removed by exposing the wafer for 2 minutes to a 600 W oxygen plasma. However, the underlying gold electrode gets slightly oxidised. Therefore after plasma cleaning the wafer was soaked for 1 hour in ethanol to reduce the oxides. Omission of this reduction step yielded upon self-assembly super-hydrophobic layers that displayed huge hysteresis in advancing and receding contact angle measurements. Similar observations have been reported previously[7, 8].

SAM formation and characterisation

The SAM coverage depends on temperature, concentration of the thiols in solution and on the incubation time[3,12]. To obtain densely packed SAMs we used an incubation time of three days. To avoid any oxidation the self-assembly took place in inert atmosphere. Alkane-mono-thiol SAMs, C_nH_{2n+1}-SH with $n = 8$-22, were assembled from 1 mM solutions in ethanol. α,ω-Alkane-di-thiols can bind on both sides with gold. To avoid formation of loops, even higher concentrations, *viz.* 3mM, were used[9,10]. We note that preliminary experiments have shown that the junction resistances decrease with lower alkanethiol concentrations and shorter incubation times. This has not been further investigated. After SAM formation the wafer is rinsed with ethanol, toluene and iso-propanol, and dried by spinning. As an empirical quality check we used complete de-wetting of the wafer by ethanol.

To demonstrate that the process technology yields densely packed SAMs, and to rule out cross contamination by the photoresists, the microstructure was investigated with XPS, Kelvin probe, contact angle and ellipsometry measurements. Due to the small surface area not all techniques can be used to study the SAM in the junctions themselves. Therefore we also separately investigated the microstructure of SAMs assembled on gold using the same process flow chart.

XPS measurements were performed to demonstrate the absence of cross contamination. The chemical composition of the SAM gradually changes with depth. We assume that the SAM can be approximated as a three layer stack *viz.* C_nH_{2n+1} / S-Au / Au. XPS peak positions yield information on the elemental composition and type of chemical bond. The XPS intensities depend on areal density and escape depth. Assuming the three layer stack the XPS measurements can be quantitatively modelled to give the SAM thickness and surface coverage[11]. The numbers derived for octadecanethiol, $C_{18}H_{37}$-SH, SAMs, as a function of cleaning procedure and proceed on bare gold and in via's are presented in Table S1.

sample	cleaning	Au (%)	C_nH_m (%)	C-O (%)	O (%)	S-O (%)	S-C (%)	S-Au (%)	Ti (%)	d (nm)	coverage (10^{14} cm^{-2})
C$_{18}$H$_{37}$SH	reference	32.1	65.7	-	-	-	0.2	1.7	-	2.4	4.4
C$_{18}$H$_{37}$SH	O$_2$	5.7	77.7	6.0	7.8	0.5	2.4	-	-	-	-
C$_{18}$H$_{37}$SH	O$_2$+EtOH	32.8	63.9	-	1.2	-	0.2	1.8	-	2.3	4.6
C$_{18}$H$_{37}$SH (L6000.5)	O$_2$+EtOH	32.3	65.8	-	-	-	0.3	1.5	-	2.3	3.7
C$_{18}$H$_{37}$SH (MA)	O$_2$+EtOH	30.2	56.4	2.7	6.7		0.6	1.8	1.7	2.3	4.3
C$_{18}$H$_{37}$SH	theory									2.3	4.6

Table S1. XPS data presented in raw concentration (at %) for different C$_{18}$H$_{37}$-SH SAMs on gold. The thickness and coverage was calculated assuming a C$_n$H$_{2n+1}$ / S-Au / Au stack. The reference sample is directly assembled on freshly evaporated gold. The SAM in second entry is assembled on oxygen plasma cleaned gold. The third SAM is assembled after a reduction step in ethanol. SAMs labelled L6000.5 and MA1407 are investigated in 50 μm via holes. The values obtained inside the via's are similar to those obtained for a SAM on bare gold. Hence cross contamination can be disregarded.

For the reference sample, octadecanethiol directly assembled on freshly evaporated gold, we find a SAM thickness and surface coverage in good agreement with theoretical values. The thickness of 2.4 nm indicates that the molecule which itself is 2.6 nm long, assembles on gold under a tilt angle of 30°. The surface coverage of 4.4×10^{14} cm^{-2} is similar to the theoretical limit[3] of 4.6×10^{14} cm^{-2}, and indicates a densely packed SAM. The second entry of Table S1 shows the detrimental influence of cleaning gold with an oxygen plasma on SAM formation. The low intensity of the gold signal in combination with the shift in the Au^{4f} peak is due to the formation of gold oxide as previously reported[7,8]. The absence of an S^{2p} peak at 161.5 eV indicates that S is not bound to Au and that no SAM is formed. As shown by the third entry, an additional reduction step by soaking the wafer 1 hour in ethanol is required. Finally we investigated SAM formation within a 50 μm *via* using the L6000.5 and MA1407 technology described above. In both cases a dense SAM is formed. We note that the small amount of Ti found using the MA1407 technology does not interfere with the SAM formation. We note that the values obtained inside the *vias* are similar to those obtained for a SAM on bare gold. Hence cross contamination can be disregarded.

The C$_n$H$_{2n+1}$-SH SAM thicknesses were independently determined from ellipsometry measurements. The thickness increases linearly with the number of carbon atoms in the backbone. The numbers indicate that the molecules assemble on gold with a tilt angle of 30° [12]. Indications for a dense packing could also be drawn from contact angle and Kelvin probe measurements. The advancing and receding contact angles are similar to values reported for perfectly ordered SAMs[3]. The workfunction for the long alkanethiol SAMs amounted to 4.1 eV, in good agreement with reported values[13]. For the shortest alkanethiol, we obtain a value of 4.34 eV. The increase in workfunction has been ascribed to more disordered dipoles within this monolayer due to the less ordered packing[12]. A summary of SAM thickness, work function and contact angle is presented for completeness in Table S2.

C_nH_{2n+1}-SH (n)	d (ellipsometry) (nm)	work function (eV)	θ_a (°)	θ_r (°)
8	0.9	4.34	111	99
10	1.26	4.18	111	100
12	1.35	4.16	112	102
14	1.61	4.16	113	102
16	1.94	4.16	114	103
18	2.3	4.17	114	103
20	2.72	4.17	114	103

Table S2. Layer thickness as derived form ellipsometry measurements, workfunction form Kelvin probe measurements, and advancing θ_a and receding contact angles θ_r for alkane-mono-thiol SAMs on gold, C_nH_{2n+1}-SH with n = 8–20.

Top electrode

The top electrode layer consists of a stack of the conducting polymer PEDOT:PSS and gold. The PEDOT"PSS is inserted to prevent top-down shorts during gold evaporation. In this electrode layer the top contacts and second layer of interconnects are defined. The lithography and subsequent process steps have been performed at room temperature. Details are presented below.

PEDOT:PSS is applied on top of the SAM as an electrically conducting barrier for the final gold top electrode. The electrical conductivity of commercial PEDOT:PSS films ranges from 0.1 S/cm to 100 S/cm. The conductivity can be enhanced by adding high boiling solvents. We added 5 % DMSO to the PEDOT:PSS batches yielding a conductivity of 300 S/cm. The water borne PEDOT:PSS does not wet the hydrophobic SAM. However, due to the large surface area on the wafer of photoresist with a contact angle of 30–40° PEDOT:PSS films can be obtained by spin coating. The PEDOT lattices are filtered over 2.7 μm and dispensed over the whole wafer. The wafer is then spun for 1 minute at 2000 rpm. The layer thickness depends on the type of PEDOT:PSS and varies between 60 nm and 140 nm. Homogenous PEDOT:PSS films were obtained when directly after spin coating the film is dried on a hot plate at 100 °C.

SAMs of alkane(di)thiols on gold are unstable at elevated temperatures. Fig. S3 shows that the advancing and receding angle of a dodecanethiol SAM decrease above about 60 °C. The inset shows the onset of deterioration as a function of carbon atoms. To avoid any thermal deterioration of the packing of the SAM we limited the process window to 50 °C. The PEDOT:PSS films therefore were not dried at elevated temperature but at room temperature in dynamic vacuum of 10^{-3} mbar. Unfortunately this drying procedure can lead to the formation of striations, *i.e.* radial thickness variations. The relation between drying conditions and resistances of the final junctions has not yet been fully investigated.
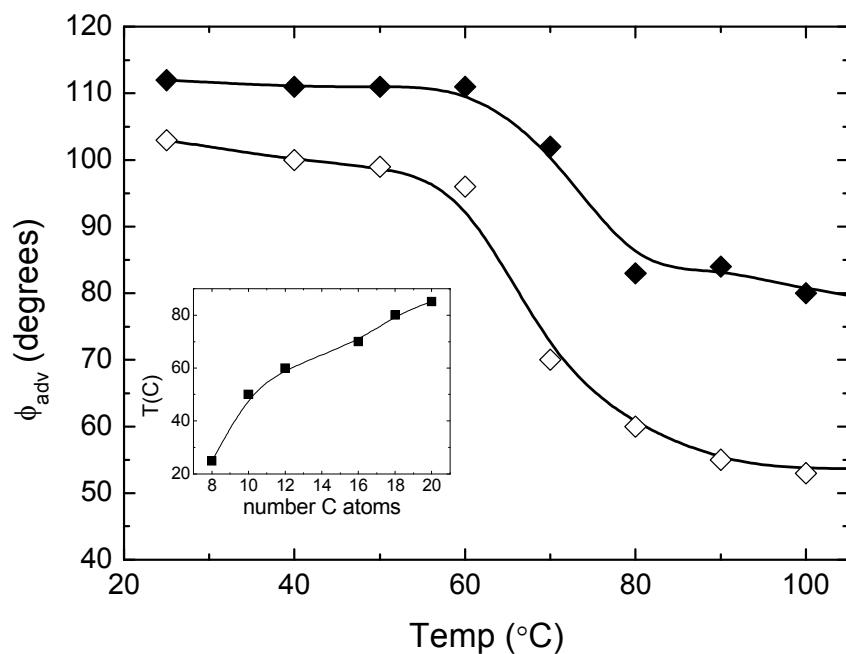
Fig. S3. Advancing (◆) and receding (◇) contact angle of a dodecanethiol SAM on gold as a function of temperature. The inset shows the onset for thermal deterioration as a function of the number of carbon atoms. The SAMs were annealed for 5 minutes in nitrogen at the given temperature. The advancing and receding contact angles were measured in ambient conditions.

The wetting of PEDOT:PSS on hydrophobic surfaces can be dramatically improved by adding surfactants to the PEDOT:PSS dispersion. Using a non-ionic, fluorinated surfactant, Zonyl FSO-100, uniform PEDOT:PSS films could be fabricated on SAMs with contact angles as large as 114°. However, the electrical resistance of the junction that is comparable to that of PEDOT:PSS-only junctions, *i.e.* junctions without a SAM. Similarly, the resistance for fluorinated SAMs, HS-C_2H_4-C_nF_{2n+1} with $n = 8$ and 10, is found to be comparable to that of PEDOT:PSS-only junctions. The origin might be intermixing of SAM and PEDOT:PSS, but this has not been further investigated.

The PEDOT:PSS was dried at room temperature in a dynamic vacuum of 10^{-3} mbar. To stay within the thermal budget, the 150 nm top gold electrode layer was not sputtered but evaporated. The top contacts and the second layer of interconnects were defined by photolithography. Pre-bake and post-bake steps were omitted. The photoresist was dried at room temperature in vacuum. Fortunately, the adhesion then is sufficient to structure the gold. Wet etching of the exposed gold with KI/I_2 yielded molecular junctions with resistances comparable to that of PEDOT:PSS-only junctions. The origin could be the diffusion of the oxidising agents through the PEDOT:PSS followed by oxidation of the SAM. To avoid this complication we abandoned wet etching and used dry argon ion etching instead. During this etching the wafer was backside cooled with helium. The end-point was determined by measuring the Au signal with a secondary ion mass spectrometer. We have not yet investigated the junction resistance as a function of process temperature

The PEDOT:PSS outside the junctions and interconnects is removed to prevent cross talk. We used reactive ion etching using a 30 W O_2 plasma. The patterned gold is used as a self-aligned mask. The reactive ion etching is not selective between PEDOT:PSS and the underlying photoresist. Therefore an optical end point determination was used. Finally the remaining photoresist on top of the gold was stripped with acetone.

Leakage currents

The leakage currents through the MA1407 and L6000.5 photoresists were determined from small signal impedance measurements on MIM capacitors integrated in the process evaluation module. The layer thickness therefore was similar to those used in actual junctions. The dielectric constants agreed with bulk values. The resistance scales with surface area. In order to compare the resistance with those of the molecular junctions we present in Fig. S4 the normalised resistance as a function of MIM device area. Fig. S4 shows that leakage currents, especially when using patterned junctions with small overlap, can be disregarded.
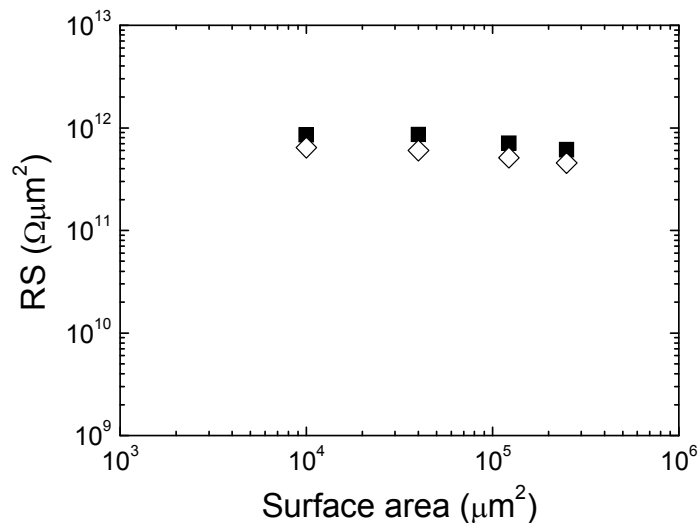

Fig. S4. Normalised resistance for MIM capacitors as a function of device area. The capacitors are integrated in the process evaluation module. The layer thickness of the MA1407 ($\diamond$) and L6000.5 ($\blacklozenge$) photoresist therefore is the same as in the actual junctions.

Device layout: Kelvin and string

We measure the electrical transport perpendicular through the SAM as elucidated in Fig. S5b. The equivalent circuit is given by discrete SAM resistors connected in parallel. Assuming that cooperative effects can be disregarded, the junction resistance then is the single molecule resistance divided by the grafting density. This interpretation is justified by a junction resistance that scales with surface area.

To eliminate the parasitic lead resistances 4-point probe measurements were performed. The layout of the Kelvin structures is presented in Fig. S5. Current is forced through opposite terminals *e.g.* 1 and 4. The potential is measured at zero current between terminals 2 and 3. The ratio then yields the device resistance.
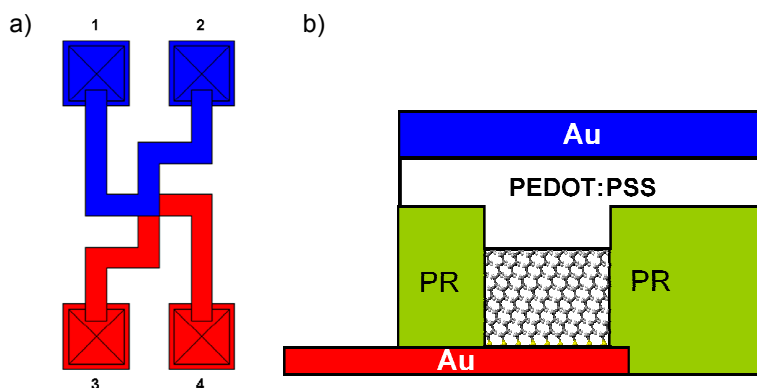

Fig. S5. (a) Layout of 4 point probe Kelvin measurement structure. Red is the bottom electrode and blue the top electrode. The diameter of the via is 5 μm (b) schematic cross section of the junction showing that transport is measured perpendicular through the SAM yielding the electrical transport properties of the single molecules.

The process technology developed comprises patterned interconnects in both top and bottom electrode layers. This allows strings to be fabricated in which a large number of molecular junctions are connected in series. The layout of strings as presented in Fig. S6a, shows that up to 100 sections, each containing two junctions, can be integrated. An optical photograph is presented in Fig. S6b. To clarify the device geometry we present in Fig. S6c a schematic vertical cross section through a part of the string. The bottom electrode is presented in red and the top electrode in blue. Fig. S6c shows 4 junctions connected in series. The current flows alternating from top to bottom.
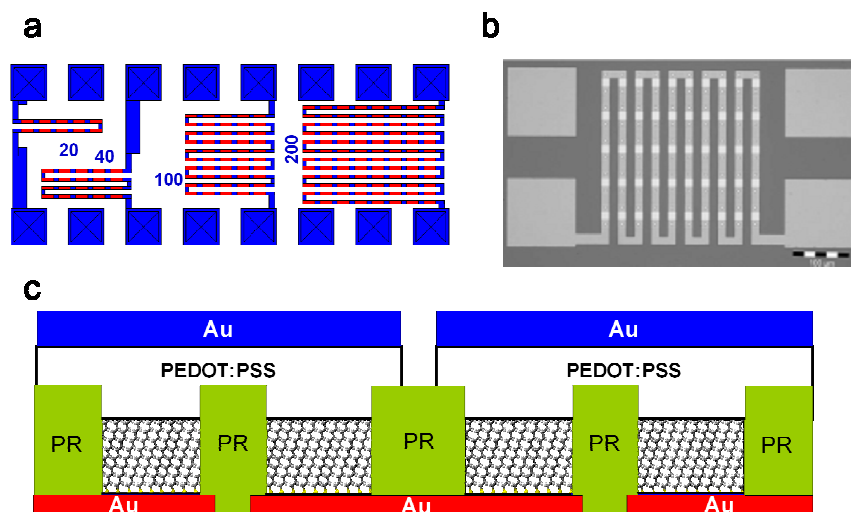

Fig. S6. Integration of molecular junctions in series. (a) Layout of strings in which a number of junctions are connected in series. Each section contains two junctions. The red and blue colour represents the bottom and top Au layers, respectively. (b) Optical

photograph of a string (c) Schematic cross section of a part of a string. The picture shows 4 junctions connected in series.

4. Electrical transport

In this section we present additional information on the electrical transport measurements of molecular junctions. First PEDOT:PSS-only junctions are addressed. As a typical example we present detailed current-voltage characteristics of alkane-mono-thiol SAM junctions. A statistical analysis of thousands of junctions is presented. Key parameters as yield and reproducibility are given. The scaling of resistance with device area is discussed and the influence of process parameters on the resistance of the molecular junctions is given.

PEDOT:PSS-only junctions

The lower limit of the resistance of the molecular junctions is given by PEDOT:PSS-only junctions, *i.e.* junctions without a SAM. PEDOT:PSS-only junctions were fabricated with PEDOT:PSS from various suppliers, with and without high boiling additives, yielding bulk conductivities between 0.1 S/cm and 300 S/cm. The normalised resistance in $\Omega\,\mu m^2$ of PEDOT:PSS-only junctions is presented as function of the laterally measured bulk PEDOT:PSS conductivity in Fig. S7.
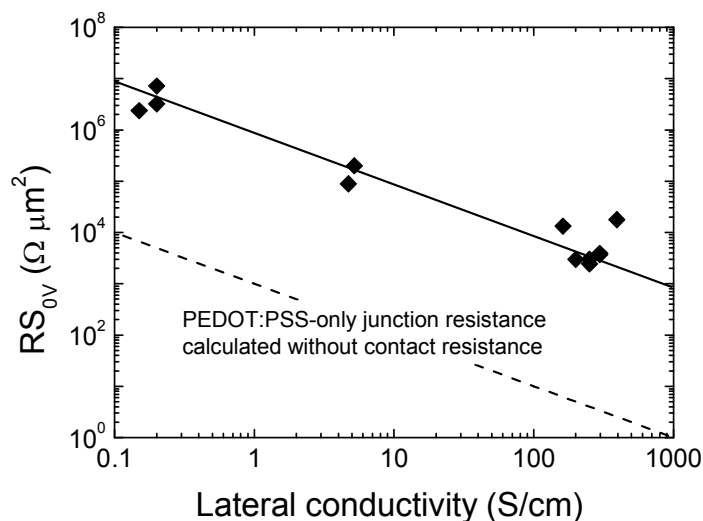

Fig. S7. Resistance of a variety of PEDOT:PSS-only junctions as a function of the laterally measured bulk conductivity. The dashed line indicates the junction resistance expected from the bulk conductivity when contact resistances can be disregarded.

The dashed line shows the junction resistance as calculated from the bulk conductivity. For all PEDOT:PSS batches studied, irrespective of supplier and or additives, the expected junction resistance is about a factor thousand lower than measured in the actual PEDOT:PSS-only junctions. We tentatively attribute this discrepancy as being due to the contact resistance at the PEDOT:PSS bottom gold contact. Electrical anisotropy is unlikely due to the length scale of the devices being

much larger than the dimensions of the primary PEDOT:PSS particles. A detailed study on thickness dependence is indicated. Scaling of the contact resistance with the bulk conductivity can be expected for electrical transport dominated by hopping of charge carriers. We note however that the proportionality constant of about a factor of thousand is large. More typical is a factor between 10 and 100.

Current-voltage characteristics of alkane-mono-thiol junctions

Typical current density - voltage characteristics of alkane-*mono*-thiol junctions C_nH_{2n+1}-SH with n = 8-22 are presented in Fig. S8. The current densities for n = 8, 10 and 12 are indistinguishable from PEDOT:PSS-only junctions. Only for the longer alkane chains the electrical transport is unambiguously dominated by the SAM.
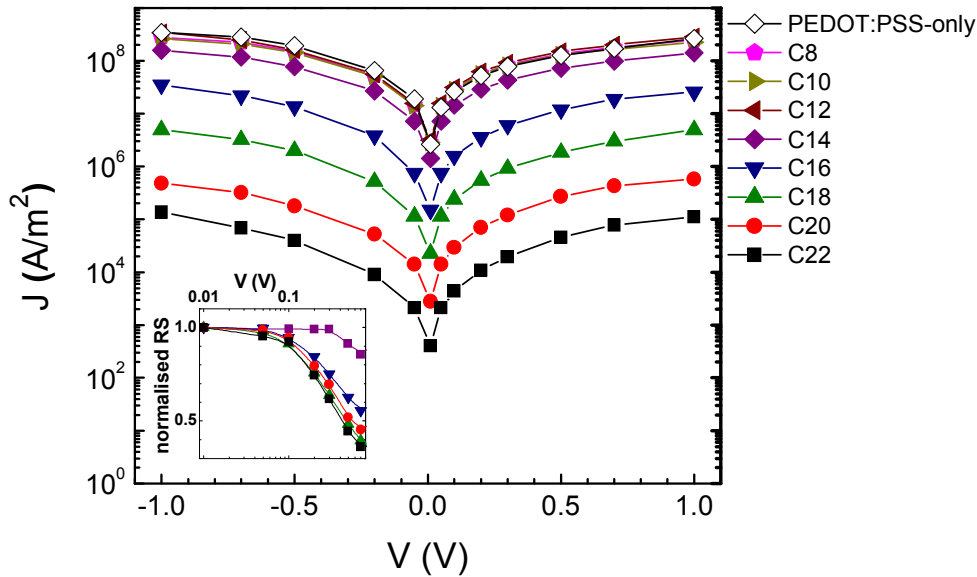

Fig. S8. Current density–voltage characteristics of alkane-mono-thiol junctions C_nH_{2n+1}-SH with n = 8–22 as processed with the default process flow chart using L6000.5 photoresist and PEDOT:PSS from Agfa. The diameter of the junction was 10 μm. The inset shows the normalised resistance as a function of bias for n = 14 - 22.

The charge transport mechanism is non-resonant tunnelling. The junction resistance is given by:

$$R = 12.9 \ k\Omega \ r_{Au-S} r_{mol} r_{SAM \ PEDOT} \tag{1}$$

where r_{Au-S}, r_{mol} and $r_{SAM \ PEDOT}$ are unitless resistance contribution factors accounting for the resistance contribution of the bottom contact, the molecule and the top contact, respectively. The molecule contribution is given by $r_{mol} = exp \ (\beta n)$, where β is the decay coefficient and n the number of carbon atoms in the backbone. The current density then exponentially decreases with increasing length. This implies that for perfect C8, C10 and C12 monothiol SAM's the junction resistance should decrease with decreasing number of carbon atoms.

This dependence could not be verified however. Experimentally we have never measured a device resistance with or without incorporated SAM lower than about

$1 \cdot 10^3$ Ohm μm^2. The reason is still not fully understood. It could be due to a small parasitic series resistance due to for instance the top gold PEDOT:PSS contact, bulk PEDOT:PSS resistance, overlap resistances, and interconnect resistances. Hence, arbitrarily, all junctions with a resistance below $1 \cdot 10^4$ Ohm μm^2 were disregarded.

The transport is symmetric and independent of temperature between –100 °C and 25 °C. The inset of Fig. S8 shows the normalised resistance as a function of bias on a logarithmic scale. At low bias the resistance is constant and with increasing bias the resistance decreases. The bias at which the nonlinearity starts, decreases with increasing alkane length. The origin might be a smaller distance between the Fermi level and the transmission peaks for the longer alkane chains. Actually thousands of junctions investigated show a universal behaviour when the nonlinearity calculated as *e.g.* R(0.5 V) / R(0.01 V) is plotted versus the normalised junction resistance (Ω μm^2).

Yield and statistical analysis

A junction is arbitrarily called electrically shorted when its normalised resistance is smaller than $1 \cdot 10^4$ Ohm μm^2 as described above. Experimentally we then find a yield of either about zero or unity. A yield of zero is obtained for fluorinated alkanethiols, for alkane-mono-thiols in combination with the use of a fluorinated surfactant in PEDOT:PSS, and when using a wet KI/I_2 etchant for the top gold electrode. In the first two cases the reason for the low yield might be intermixing of SAM and PEDOT:PSS. The reason for formation of shorts upon wet etching the gold top electrode might be diffusion of the oxidising agents through the PEDOT:PSS layer followed by oxidation of the SAM.

Typically however, the yield is about unity. Apparently the technology is robust against imperfections in the SAM. We note that the bottom gold electrode is polycrystalline. The root mean square roughness of 0.5 – 1 nm is only slightly smaller than the length of the molecules, about 2 – 3 nm. The SAM layer is ordered but not single crystalline. The monolayer contains a large number of structural defects distributed on a length scale smaller than the diameter of the junctions. The defects however do not lead to shorts. The reason is related to the difference in surface tension between the SAM and PEDOT:PSS. The poor wetting prevents intermixing. Consequently, PEDOT:PSS forms a badly adhering, continuous film on top of the SAM. The tolerance of our technology for SAM defects is supported by transport measurements on long α,ω-alkane-*di*-thiols. XPS analyses of HS-$C_{14}H_{28}$-SH SAMs showed the presence of both standing-up, lying-down and looped phases[10]. Each phase has a different effective tunnelling length. The overall junction resistance therefore depends on the composition. Despite these inhomogeneities however, the PEDOT:PSS layer remains continuous and the junctions are not shorted.

A histogram of the normalised resistance for a series of even alkane-mono-thiols C_nH_{2n+1}-SH with n =14 - 22 is shown in Fig. S9. One wafer was fabricated for each molecule. However for C_{18}, 4 wafers yielding 1708 discrete devices were analysed. The resistance of C_{20} and C_{22} monothiols junctions with device diameter smaller than 4 μm were too high to be reliably determined. Therefore they were omitted in Fig. S9. As a comparison, the statistical data for PEDOT:PSS-only junctions are included.

Fig. S9 shows that the average normalized resistances increase with number of carbon atoms in agreement with Eq.(1). The small standard deviation indicates the reproducibility of device fabrication.
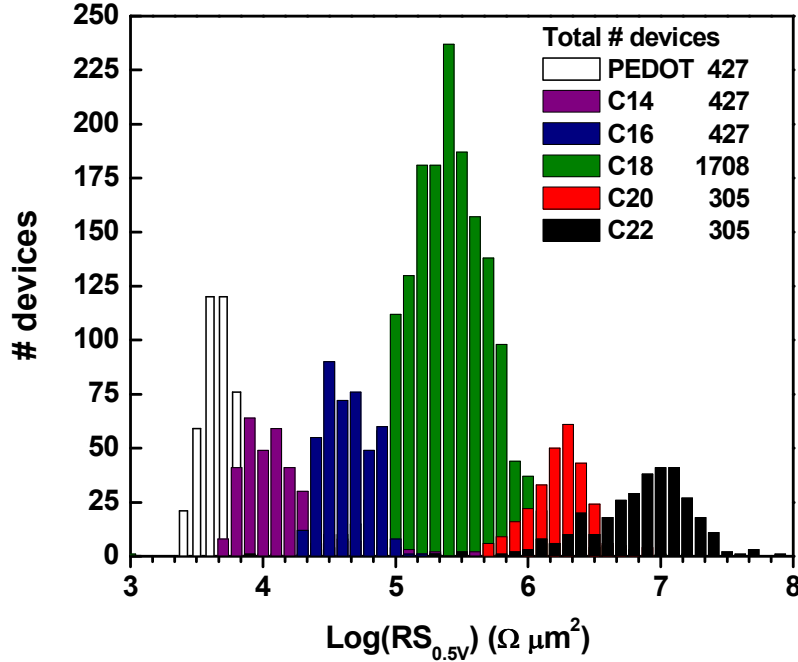

Fig. S9. Histogram of the normalised resistance for the series of even alkane-mono-thiols C_nH_{2n+1}-SH with n =14 - 22 using the default process flow chart. The data for PEDOT:PSS-only junction are included for comparison.

Scaling of resistance with device area

We measure the electrical transport perpendicular through the SAM. When cooperative effects can be disregarded, the equivalent circuit is given by discrete SAM resistors connected in parallel. This implies that the resistance should scale with device area. As a typical example the normalised resistances and their standard deviation of a $C_{18}H_{37}$-SH SAM junction are presented in Fig. S10 as function of junction area. In first approximation the data show perfect scaling meaning that the normalised resistance does not depend on device area. Deviations for the smallest junction with an area of 1 μm^2 are presumably due to spatial resolution of the negative photoresist. A closer inspection however shows a small but systematic deviation. Fig. S10 shows that for larger areas the change in average resistance is about a factor of three, significantly larger than the standard deviation.

The scaling can be explained by factorisation of the electrical transport. As shown in Eq. (1) the junction resistance depends on the product of the unitless resistance contribution factors accounting for the resistance contribution of the bottom contact, r_{Au-S}, the molecule, r_{mol}, and the top contact, $r_{SAM\ PEDOT}$. PEDOT:PSS forms a physisorbed contact on the SAM. Small variations in the microstructure such as bonding distances lead to significant changes in the electronic coupling and, hence, to large variations in the top contact resistance factor, $r_{SAM\ PEDOT}$. This variation in $r_{SAM\ PEDOT}$ can explain the non-perfect scaling of the resistance with junction diameter and the offset in junction resistance when changing the processing. Crucial is processing

of PEDOT:PSS because it does not adhere to the SAM. Homogeneous PEDOT:PSS films could be made by careful adjustment of the processing conditions such as dispensing the solution over the whole 150-mm wafer and immediate drying of the film after spin coating. To study the influence of PEDOT:PSS processing on junction resistance we deliberately deposited inhomogeneous films with large thickness variations. On a single wafer the variation in resistance could be orders of magnitude. Mapping the junction resistance with the PEDOT:PSS thickness showed a one to one correspondence; the thicker the PEDOT:PSS film the lower the junction resistance. We tentatively explain this relation as being due to a more intimate SAM / PEDOT:PSS contact for the thicker PEDOT:PSS films leading to a smaller top contact resistance factor, $r_{SAM\ PEDOT}$.
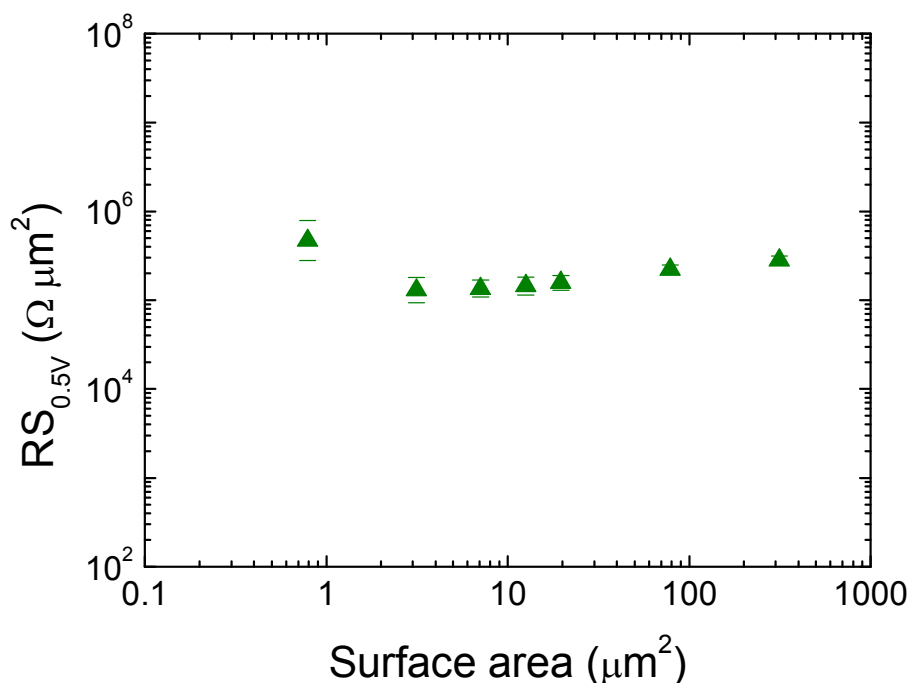

Fig. S10. Normalised resistances in $\Omega\,\mu m^2$ and their standard deviations of a $C_{18}H_{37}$-SH SAMs junctions as a function of surface area.

The molecular junctions are enclosed in *vias* of photoresist. The surface tension of the photoresist is different from that of the SAM with the SAM being much more hydrophobic and the contact angles differing by more than 80°. The waterborne PEDOT:PSS adheres better to the photoresist than to the SAM. Consequently the local electrical resistance varies over the junction; being lower at the edge than in the middle of the junction. The final result is a resistance that does not perfectly scale with surface area as shown in Fig. S10.

Finally, we note that for very small *vias* with a diameter of 2 μm or less the opposite behaviour is found. The reason however is the same. The *vias* are now so small that due to capillary forces the PEDOT:PSS cannot wet the SAM. The normalised resistance then increases with decreasing junction diameter.

Influence process parameters on junction resistance

17

The normalised resistance of the alkane-mono-thiol SAM junctions are presented in Fig. S11 as a function of the number of carbon atoms. The dotted line represents the PEDOT:PSS-only value. The red diamonds represent devices made with the standard technology. The blue dots represent junctions made with a different type of PEDOT:PSS. The green squares represent the averaged normalised resistances when MA1407 photoresist is used instead of L6000.5. The three solid lines represent a fit to the data points. Fig. S11 shows that the resistance is factorised according to Eq. (1). The resistance increases exponentially with the length with a decay constant β calculated as 0.9 per carbon atom, which corresponds to 0.73 Å^{-1}. The absolute values differ by an offset set by the technology, but the decay constants are comparable. The offset is determined by the technology via $r_{SAM\ PEDOT}$ that is a measure of the electronic coupling strength between the SAM and PEDOT:PSS. We note that the interpretation is only phenomenological. A microscopic explanation for the dependence of the electronic coupling of the top contact cannot be presented.
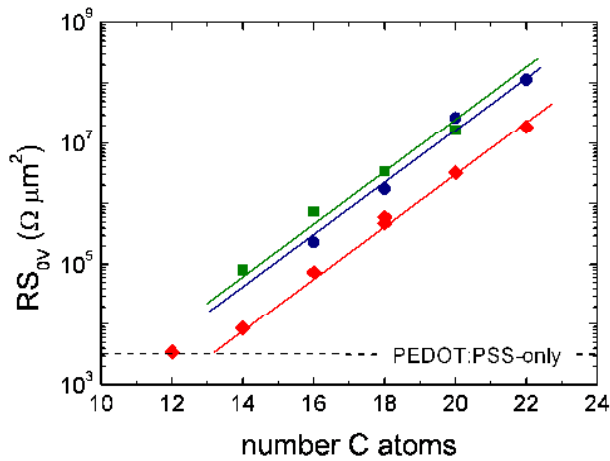

Fig. S11. Resistance as a function of process parameters. The normalised resistance of alkane-mono-thiol C_nH_{2n+1}-SH SAM junctions with n = 14 – 22, averaged over all junctions on the wafer, on a semi-logarithmic scale as a function of the number of carbon atoms in the alkanethiol backbone, n. The dotted line represents the PEDOT:PSS-only value. The red diamonds (◆) represent devices made with the default process flow chart using L6000.5 as a photoresist and with PEDOT:PSS from Agfa (ICP new-type) that contains 5 vol % DMSO. The blue dots (●) represent the averaged normalised junction resistances when using a different type of PEDOT:PSS, PH500 with 5 % DMSO. The green squares (■) represent the averaged normalised resistances when MA1407 photoresist is used instead of L6000.5. The three solid lines represent a fit to the data points. The resistance of the alkanethiol SAM junctions increases exponentially with the length according to RS ~ exp (β n) with decay constant β calculated as 0.9 per carbon atom, which corresponds to 0.73 Å^{-1}. The absolute values differ by an offset set by the technology, but the decay constants are comparable.

Apart from the alkane-mono-thiol SAMs, also α,ω–alkane-di-thiol SAMs were investigated. We found a similar factorisation of electrical transport, but with larger processing variations.

The normalised resistances are presented in Fig. S12. The red diamonds represent α,ω-alkane-di-thiol $HS-C_nH_{2n}-SH$ SAM junctions fabricated using the standard technology. The green spheres represent reported values for discrete α,ω-alkane-di-thiol junctions[1]. Fig. S12 shows that the decay coefficients are comparable but there is an offset in absolute values of a factor of thousand. To address this discrepancy we fabricated C12 dithiol SAM junctions where we deliberately varied the type of photoresist, composition and processing of PEDOT:PSS and the gold cleaning procedures. The resistance values obtained are included as the black triangles in Fig S12. These resistances bridge the gap between the standard technology and the previously published values. The reason is not yet fully understood. To demonstrate that each technology changes the offset but yields a comparable decay coefficient, the length dependence has to be determined which has not been attempted.
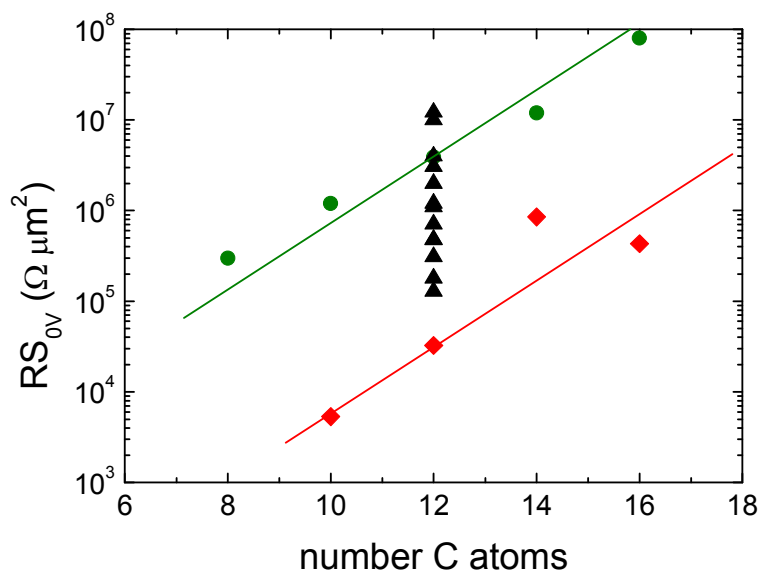

Fig. S12. The red diamonds (◆) represent the normalised resistance of α,ω-alkane-di-thiol $HS-C_nH_{2n}-SH$ SAM junctions with n = 10 - 16, averaged over all junctions on the wafer, on a semi-logarithmic scale as a function of the number of carbon atoms in the α,ω-alkane-di-thiol backbone, n, using the default process flow chart. The green spheres (●) represent the reported values for discrete α,ω-alkane-di-thiol junctions[1] Resistance values for C12 dithiol SAM junctions where the type of photoresist, type and processing of PEDOT:PSS and the gold cleaning procedures have been varied are included as well (▲). These resistances bridge the gap between the default process flow chart and reported values.

References

1.   Akkerman, H. B., Blom, P. W. M., de Leeuw, D. M. & de Boer, B. Towards Molecular Electronics with Large-Area Molecular Junctions. *Nature* **441**, 69-72 (2006).

2.   Hansen, W. N. & Hansen, G. J. Standard Reference Surfaces for Work Function Measurements in Air. *Surf. Sci.* **481**, 172-184 (2001).

3.   Bain, C. D., *et al.* Formation of Monolayer Films by the Spontaneous Assembly of Organic Thiols from Solution onto Gold. *J. Am. Chem. Soc.* **111**, 321-335 (1989).

4.   Loh, W. M., Swirhun, S. E., Schreyer, T. A., Swanson, R. M. & Saraswat, K. C**.** Modeling and Measurement of Contact Resistances. *IEEE Trans. on Electron Devices* **34**, 512-524 (1987).

5.   Hen, J. & Lindsay, S. M. On the Mechanism of Negative Differential Resistance in Ferrocenylundecanethiol Self-Assembled Monolayers. *J. Am. Chem. Soc.* **127**, 11932-11933 (2005).

6.   de Brito, B. C. *et al.* Ultra Low Power Microfuses for Write-Once Read-Many Organic Memory Elements. *Adv Mater* in press (2008).

7.   Ron, H. & Rubinstein, I. Alkanethiol Monolayers on Preoxidized Gold. Encapsulation of Gold Oxide under an Organic Monolayer. *Langmuir* **10**, 4566-4573 (1994).

8.   Ron, H., Matlis, S. & Rubinstein, I. Self-Assembled Monolayers on Oxidized Metals. 2. Gold Surface Oxidative Pretreatment, Monolayer Properties, and Depression Formation. *Langmuir* **14**, 1116-1121 (1998).

9.   Kohale, S., Molina, S.M., Weeks, B.L., Khare, R. & Hope-Weeks, L.J. Monitoring the Formation of Self-Assembled Monolayers of Alkanedithiols Using a Micromechanical Cantilever Sensor. *Langmuir* **23,** 1258-1263 (2007).

10.   Akkerman, H. B. *et al.* Self-Assembled-Monolayer Formation of Long Alkanedithiols in Molecular Junctions. *Small* **4**, 100-104 (2008).

11.   van der Marel, C., Yildirim, M. & Stapert, H. R**.** Multilayer Approach to the Quantitative Analysis of X-ray Photoelectron Spectroscopy Results: Applications to Ultrathin SiO_2 on Si and to Self-Assembled Monolayers on Gold. *J. Vac. Sci. Technol. A* **23**, 1456-1470 (2005).

12.   Ulman, A., (ed.) *Self-Assembled Monolayers of Thiols*. (Academic Press, San Diego, CA, 1998 Vol.24).

13.   de Boer, B., Hadipour, A., Mandoc, M. M., van Woudenbergh, T. & Blom, P. W. M. Tuning of Metal Work Functions with Self-Assembled Monolayers. *Adv. Mater.* **17**, 621-625 (2005).